Nuclear Engineering and Design 47 (1978) 305–315

ENDOCHRONIC MODEL FOR NONLINEAR TRIAXIAL BEHAVIOR OF CONCRETE

Zdeněk P. BAŽANT and Ching-Long SHIEH
Department of Civil Engng., Northwestern University, Evanston, Illinois 60201, USA.

Received 10 March 1977

A gradual accumulation of inelastic strain can be most conveniently described in terms of the so-called intrinsic time, whose increment depends on the time increment as well as the strain increments, and was originally developed for metals and was extended in a previous paper by Z.P. Bažant to concrete. In that previous paper it had been demonstrated that the proposed model predicts quite closely: (1) Stress-strain diagrams for concretes of different strength; (2) uniaxial, biaxial and triaxial stress-strain diagrams and failure envelopes; (3) failure envelopes for combined torsion and compression: (4) lateral strains and volume expansion in uniaxial and biaxial tests; (5) the behavior of spirally confined concrete; (6) hysteresis loops for repeated high compression: (7) cyclic creep up to 10^6 cycles; (8) the strain rate effect; (9) the decrease of long time strength: and (10) the increase of short-time strength due to low stress creep.

The present paper presents a refinement of the endochronic theory of concrete which consists mainly in taking into account; (a) the inelastic strains due to hydrostatic compression; (b) improved descriptions of strain-softening behavior, (c) cyclic loading in strain-softening range, and (d) volume change in strain-softening range; (e) the differences between proportional and standard triaxial tests; (f) triaxial failure envelopes; and (g) dependence of material parameters on strength. The formulation consists fully of continuous functions, and for numerical analysis it has the advantage that it contains no inequalities.

The present expressions are, admittedly, rather complicated and contain many parameters. However, for computer calculations this is not an insurmountable drawback. The agreement with test data is far superior to any other constitutive law found this far – virtually all currently known basic properties are modeled. The value of all material parameters are given, their dependence on concrete strength is identified, and a broad range of normal weight concrete is covered.

1. Introduction and objectives

In prestressed concrete reactor vessels, concrete is subjected generally to triaxial stresses. This is a distinct feature by which the state of stress in concrete differs from that in most other structures, such as frames, slabs and shells, in which the stress state is predominantly uniaxial or biaxial. Thus, it is particularly for failure analysis of reactor vessels that a mathematical model for nonlinear triaxial behavior of concrete is needed.

The mathematical model which presently appears to be most powerful is the endochronic theory, which has been presented in refs. [1–4]. In this theory, the inelastic strains are characterized by means of increments of intrinsic time, a non-decreasing scalar variable whose increments depend on strain increments. This concept was first introduced in practical triaxial constitutive relations by Valanis [5], who also coined the term "endochronic". Compared to the original applications of endochronic theories for metals [5], the formulation for concrete [2] is distinguished chiefly by hydrostatic pressure sensitivity of inelastic strain, by inelastic dilatancy due to large deviatoric strains, and by strain-softening. The endochronic theory [2] has been shown to give a good fit of basic known experimental data on multiaxial nonlinear behavior of concrete, including uniaxial, biaxial and triaxial tests, torsion compression tests, lateral strains, strain-softening branches and failure envelopes, spirally confined concrete, unloading, reloading and cyclic loading (up to 4×10^6 cycles) and effects of load duration and loading rate. The prediction capability of the theory has been demonstrated for cyclic moment-curvature relationships for reinforced concrete members [3]. The formulation from ref. [2] has been or is being incorporated in several finite element codes around the world.

The purpose of this paper is to present the results

of an extremely tedious and time-consuming analysis of further test data which resulted in a significant refinement of the endochronic theory from ref. [2]. This refined formulation is ready for being used in finite element programs.

2. Proposed stress–strain relations

The elastic properties are assumed to be incrementally isotropic, and, accordingly, the stress–strain relations are conveniently written in terms of separate deviatoric and volumetric relations:

$$de_{ij} = \frac{ds_{ij}}{2G} + de''_{ij}\,, \qquad de''_{ij} = \frac{s_{ij}}{2G}\,dz$$

$$d\epsilon = \frac{d\sigma}{3K} + d\epsilon''\,,$$

$$d\epsilon'' = d\epsilon^0 + d\lambda + \frac{\sigma}{3K}dz' + d\lambda' \tag{1}$$

in which $e_{ij} = \epsilon_{ij} - \delta_{ij}\epsilon$ = deviatoric components of strain tensor ϵ_{ij}, $\epsilon = \frac{1}{3}\epsilon_{kk}$ = volumetric strain, δ_{ij} = Kronecker delta, $s_{ij} = \sigma_{ij} - \delta_{ij}\sigma$ = deviatoric components of stress tensor σ_{ij}, $\sigma = \frac{1}{3}\sigma_{kk}$ = volumetric stress (negative for compression), subscripts i, j refer to Cartesian coordinates x_i ($i = 1, 2, 3$), ϵ^0 = stress-independent inelastic strain, such as thermal dilatation or shrinkage, and K, G = bulk and shear modulus which depend on λ. Furthermore, e''_{ij} = inelastic deviator strain, λ = inelastic dilatancy, λ' = shear compaction, and z and z' are intrinsic times for distortion and compaction, respectively;

$$dz = \left[\left(\frac{d\zeta}{Z_1}\right)^2 + \left(\frac{dt}{\tau_1}\right)^2\right]^{1/2},$$

$$d\zeta = \frac{d\eta}{f(\eta, \boldsymbol{\varepsilon}, \boldsymbol{\sigma})}, \qquad d\eta = F(\boldsymbol{\varepsilon}, \boldsymbol{\sigma})\,d\xi \tag{2}$$

$$dz' = \left[\left(\frac{d\zeta'}{Z_2}\right)^2 + \left(\frac{dt}{\tau_1}\right)^2\right]^{1/2},$$

$$d\zeta' = \frac{d\eta'}{h(\eta')}\,, \qquad d\eta' = H(\boldsymbol{\sigma})\,d\xi'\,, \tag{3}$$

$$d\xi = \sqrt{J_2(d\boldsymbol{\varepsilon})} = \sqrt{\tfrac{1}{2}\,de_{ij}de_{ij}}\,,$$
$$d\xi' = \sqrt{[I_1(d\boldsymbol{\varepsilon})]^2} = |d\epsilon_{11} + d\epsilon_{22} + d\epsilon_{33}|\,, \tag{4}$$

$$d\lambda = l(\lambda)\,L(\lambda, \boldsymbol{\varepsilon}, \boldsymbol{\sigma})\,d\xi\,, \qquad d\lambda' = l'(\lambda')\,L'(\lambda'\ \boldsymbol{\varepsilon}, \boldsymbol{\sigma})\,d\xi\,. \tag{5}$$

Here J_2 = second invariant of the deviator of the tensor which follows in parentheses, I_1 = first invariant of the tensor which follows; Z_1, τ_1 = constants; $f(\eta, \boldsymbol{\varepsilon}, \boldsymbol{\sigma})$ = distortion hardening function, $F(\boldsymbol{\varepsilon}, \boldsymbol{\sigma})$ = distortion softening function, $h(\eta')$ = compaction hardening function, $H(\boldsymbol{\sigma})$ = compaction softening function, $l(\lambda)$ = dilatancy function, $L(\lambda, \boldsymbol{\varepsilon}, \boldsymbol{\sigma})$ = dilatancy softening function; ξ and ξ' = non-decreasing scalar variables called distortion measure and compaction measure. In what follows, consideration will be given only to the case of sufficiently rapid deformation, for which $d\zeta/dt \gg 1$ and $d\zeta'/dt \gg 1$, so that the time-dependent terms in dz and dz' become negligible, i.e.,

$$dz = d\zeta/Z_1\,, \qquad dz' = d\zeta'/Z_2\,,$$
(rapid deformation) (6)

and the intrinsic time is independent of time per se.

By analysis of test data the following hardening and softening functions have been identified:

$$f(\eta, \boldsymbol{\varepsilon}, \boldsymbol{\sigma}) = \left(1 + \frac{\beta_1\eta + \beta_2\eta^2}{1 + F_2/a_7)}\right)F_3\,,$$

$$F_3 = 1 + \frac{a_{10}}{J_2(\boldsymbol{\varepsilon})(1 + a_9/\eta^2)}\,, \tag{7}$$

$$F(\boldsymbol{\varepsilon}, \boldsymbol{\sigma}) = F_1 + F_2\,, \quad F_1 = \frac{a_0(1 - g_1)}{1 - a_5(I_3^\sigma)^{1/3}(1 + g_2)}, \tag{8}$$

$$F_2 = [a_2\sqrt{J_2(\boldsymbol{\varepsilon})}(1 + |a_6 I_2^\sigma|^{1/4} + F_5)]/[1 - a_1 I_1(\boldsymbol{\sigma}) + |a_8 I_2^\sigma|^{1/4}F_4 - a_3 I_3(\boldsymbol{\sigma})[J_2(\boldsymbol{\sigma})]^{1/8}(1 + g_2)]\,, \tag{9}$$

$$g_1 = g_{11}g_{12}\,, \quad g_2 = g_{21}g_{22}g_{23}\,,$$

$$g_{12} = 1 - \left[1 + \left(\frac{\sigma_{\min}}{a_{17}(\sigma_{\max} - a_{23})}\right)^4\right]^{-1} \tag{10}$$

$$g_{11} = a_{14}\,[J_2(\boldsymbol{\varepsilon})]^{1/4}\,\frac{\sigma_{\text{med}} - \sigma_{\min}}{\sigma_{\max} - a_{23}}$$
$$\times\left[a_{15}\left(\frac{\sigma_{\text{med}} - \sigma_{\min}}{\sigma_{\max} - a_{23}}\right)^{4/3} - a_{16}\right]\,, \tag{11}$$

$$g_{21} = \left[\frac{a_{18}\left(\frac{\sigma_{med} - \sigma_{min}}{\sigma_{med} - a_{23}}\right) - 1}{a_{19}\left(1 - a_{20}\frac{|\sigma_{min}|}{\sigma_{max} - a_{23}}\right)(\sigma_{min} - a_{23})} \right]^{5/4},$$

$$g_{22} = \left[1 + a_{21}\left(\frac{\sigma_{min}}{\sigma_{max} - a_{23}}\right)^4\right]^{-1}, \quad (12)$$

$$g_{23} = \left(\frac{[J_2(\varepsilon)]^{1/4}}{a_{22} + [J_2(\varepsilon)]^{1/2}}\right)^3, \quad F_4 = \left(\frac{[J_2(\varepsilon)]^{1/4}}{a_4 + [J_2(\varepsilon)]^{1/2}}\right)^3, \quad (13)$$

$$F_5 = a_{11}\sigma_{min}(1 + a_{12}\sigma_{min})\left(\frac{[J_2(\varepsilon)]^{1/4}}{|a_{13}\sigma_{min}|^{1/4} + [J_2(\varepsilon)]^{1/2}}\right)^3, \quad (14)$$

$$h(\eta') = 1 + \frac{\eta'}{\beta_3} + \left(\frac{\eta'}{\beta_4}\right)^2, \quad H(\boldsymbol{\sigma}) = b_1\left(\frac{I_1(\boldsymbol{\sigma})}{b_2 - I_1(\boldsymbol{\sigma})}\right)^2, \quad (15)$$

$$l(\lambda) = 1 - \frac{\lambda}{\lambda_0},$$

$$L(\lambda, \boldsymbol{\varepsilon}, \boldsymbol{\sigma}) = \frac{c_3}{1 - c_1 I_1(\boldsymbol{\sigma})}\left[\left(\frac{\lambda}{\lambda_0}\right)^2 + \left(\frac{c_4 J_2(\varepsilon)}{c_2^2 + J_2(\varepsilon)}\right)^2\right], \quad (16)$$

$$G = \frac{1}{1 + c_5\lambda}\frac{E_0}{2(1+\nu)}, \quad K = \frac{1}{1 + c_5\lambda}\frac{E_0}{3(1-2\nu)}, \quad (17)$$

$$l'(\lambda') = c_6\left(1 - \frac{|\lambda'|}{\lambda_0'}\right), \quad L'(\lambda', \boldsymbol{\varepsilon}, \boldsymbol{\sigma}) = \frac{\sigma_{min} g_3^{1/3}}{1 + |g_3/c_8|^3},$$

$$g_3 = |c_7\sigma_{min}|0.93 - \sqrt{J_2(\varepsilon)}, \quad (18)$$

in which E_0, ν, a_0, a_1, ... a_{23}, b_1, b_2, c_1, ... c_8, β_1, ... β_4, λ_0, λ_0', Z_1, Z_2 are material parameters; I_3 = third invariant of the tensor which follows in parentheses; σ_{max}, σ_{min} and σ_{med} = maximum, minimum and medium principal stresses, the maximum being considered in the sense of compression, i.e., $\sigma_{max} \leqslant \sigma_{med} \leqslant \sigma_{min}$.

The material parameters have been identified by fitting of test data using the same method as previously [2]. The dependence of the parameters upon strength f_c' has been also established more accurately. The results of this extremely tedious and time-consuming work are the following values of material parameters, applicable for usual normal weight concretes of strength 3000 to 7000 psi (20.7 to 48.3 MN/mm^2, with 1 psi = 6.89 kN/m^2):

$$a_0 = 0.7, \quad a_1 = \frac{0.6}{f_c'},$$

$$a_2 = 1400\left(\frac{f_c'}{4650\text{ psi}}\right)^{1/2}, \quad a_3 = \frac{90}{f_c'^3}\left(\frac{3600\text{ psi}}{f_c'}\right),$$

$$a_4 = 0.045, \quad a_5 = \frac{0.6}{f_c'}\left(\frac{3600\text{ psi}}{f_c'}\right), \quad a_6 = \frac{0.15}{f_c'^2},$$

$$a_7 = 0.05, \quad a_8 = \frac{15}{f_c'^2}\left(\frac{f_c'}{3600}\right)^{1.5}, \quad a_9 = 1.5 \times 10^{-3},$$

$$a_{10} = 1.25 \times 10^{-4}, \quad a_{11} = \frac{0.2}{f_c'},$$

$$a_{12} = \frac{0.8}{f_c'}, \quad a_{13} = \frac{2.2 \times 10^{-5}}{f_c'},$$

$$a_{14} = 25, \quad a_{15} = 1.095, \quad a_{16} = 1.216,$$

$$a_{17} = 0.055, \quad a_{18} = 0.94, \quad (19)$$

$$a_{19} = \frac{1.0}{f_c'}\left(\frac{6300\text{ psi}}{f_c'}\right), \quad a_{20} = 14, \quad a_{21} = 1000,$$

$$a_{22} = 0.04, \quad a_{23} = 0.2 f_c',$$

$$b_1 = 9.1\left(\frac{f_c'}{7020\text{ psi}}\right), \quad b_2 = 1.0 f_c', \quad c_1 = \frac{2.0}{f_c'},$$

$$c_2 = 3.0 \times 10^{-3}, \quad c_3 = 0.5, \quad c_4 = 2.0,$$

$$c_5 = 150, \quad \beta_1 = 30, \quad \beta_2 = 3500,$$

$$\beta_3 = 0.08, \quad \beta_4 = 0.23, \quad Z_1 = 0.0015,$$

$$Z_2 = 0.0125, \quad \lambda_0 = 0.003, \quad \nu = 0.18,$$

$$c_6 = 0.002/\text{psi}, \quad c_7 = 1.05 \times 10^{-6}/\text{psi},$$

$$c_8 = 0.001, \quad \lambda_0' = 0.003,$$

$$E_0 = 4 \times 10^6\text{ psi} + (f_c' - 4650\text{ psi})10^3.$$

It must be pointed out, however, that the dependence of all parameters on a single experimental parameter, strength f_c', is a simplification. It is known [6] that it is possible to prepare concrete mixtures giving the same strength f_c' but rather a different initial elastic modulus E_0. The most blatant example of this is given in part III of Waterways Experiment Station Report

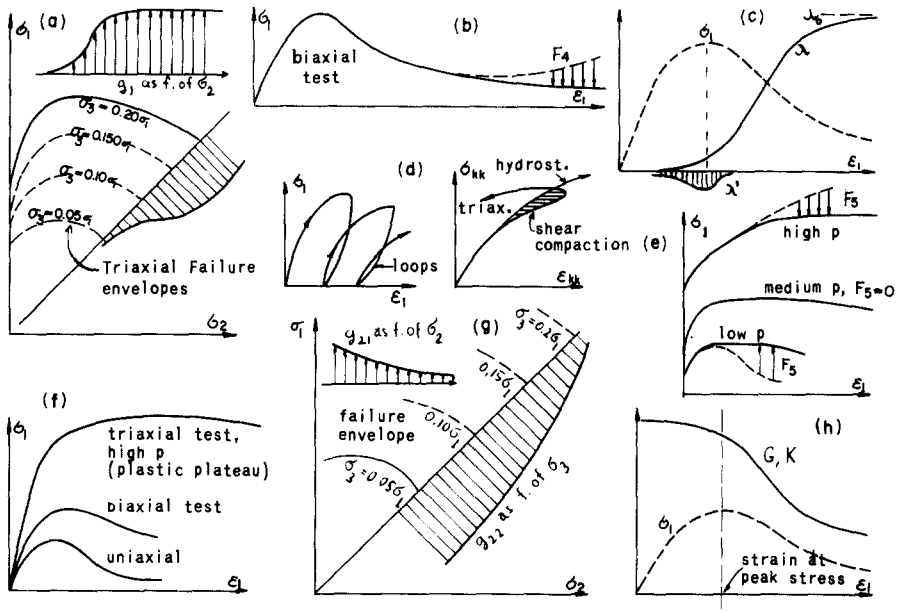

Fig. 1. Effect of various coefficients in the hardening and softening functions.

[6], in which E_0-values of 6.70, 5.82, and 3.02×10^6 psi are indicated for three mixtures giving the same strength. However, for usual mixtures, the assumption that the relationship of E_0 to f_c' is unique is an acceptable approximation. The formula which has worked best for the relationship of E_0 to f_c' is different from the ACI formula as well as the CEB-FIP formula, but the differences in predicted E_0-values are not too significant.

The fits of various test data obtained with indicated material parameters are shown in figs. 2–12.

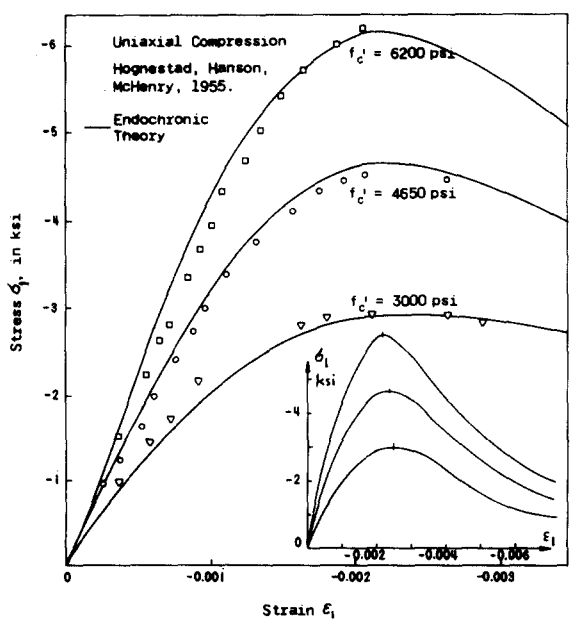

Fig. 2. Fit of uniaxial test data of hognestad, hanson and mchenry.

3. Analysis of proposed stress-strain relations

To avoid repetition of lengthy arguments and discussions, interested reader should consult ref. [2] for derivation of the basic form of the constitutive equa-

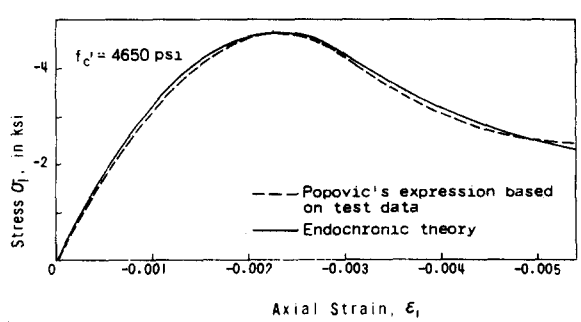

Fig. 3. Fit of popovics' expression for complete stress–strain curve representing an average of various test data.

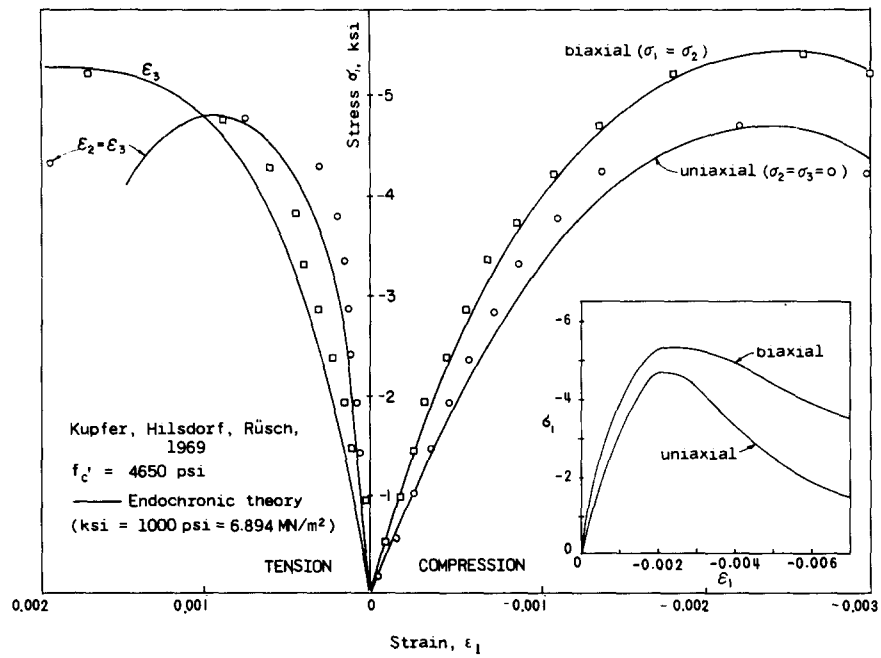

Fig. 4. Fit of axial and lateral strains in uniaxial and biaxial tests of Kupfer hilsdorf and Rüsch.

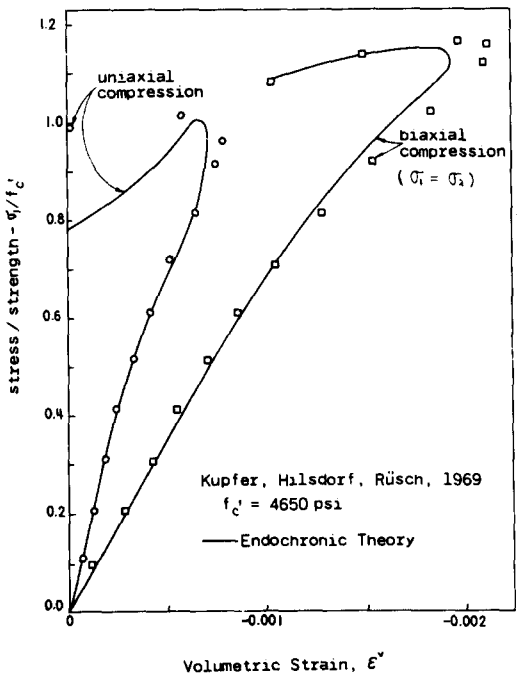

Fig. 5. Fit of volume change diagrams for uniaxial and biaxial tests of Kupfer, Hilsdorf and Rüsch.

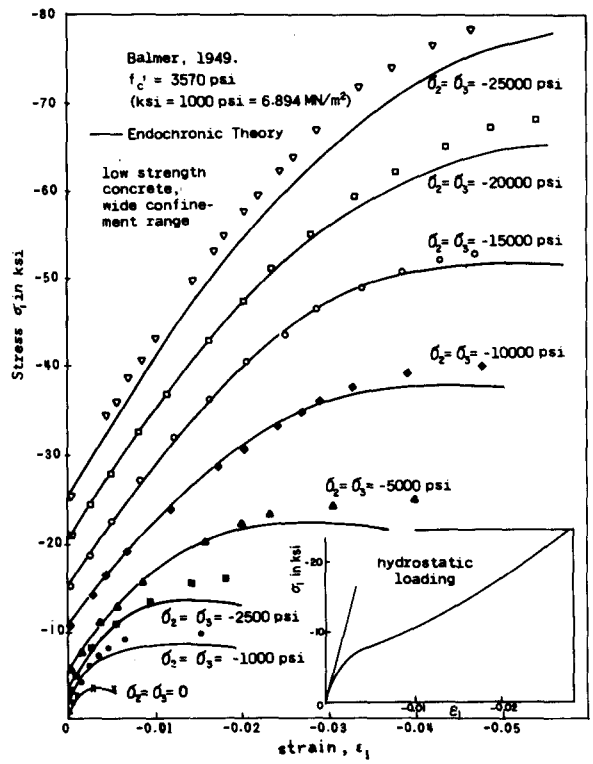

Fig. 6. Fit of triaxial test data of Balmer for low strength concrete with a broad range of confining pressures (data points on hydrostatic loading are unavailable).

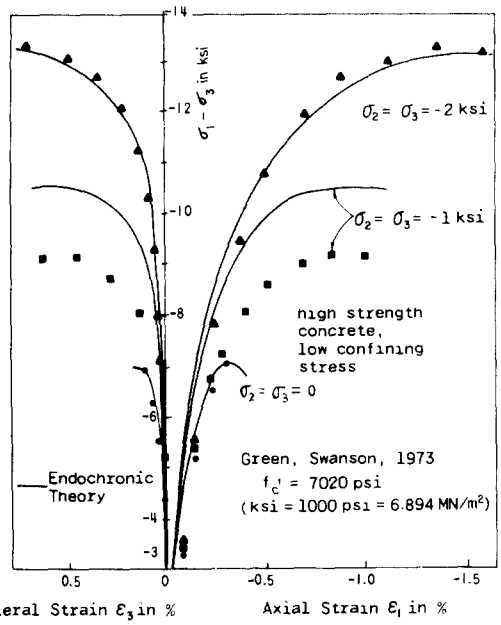

Fig. 7. Fit of triaxial test, Green and Swanson's data for high strength concrete at low confining pressures.

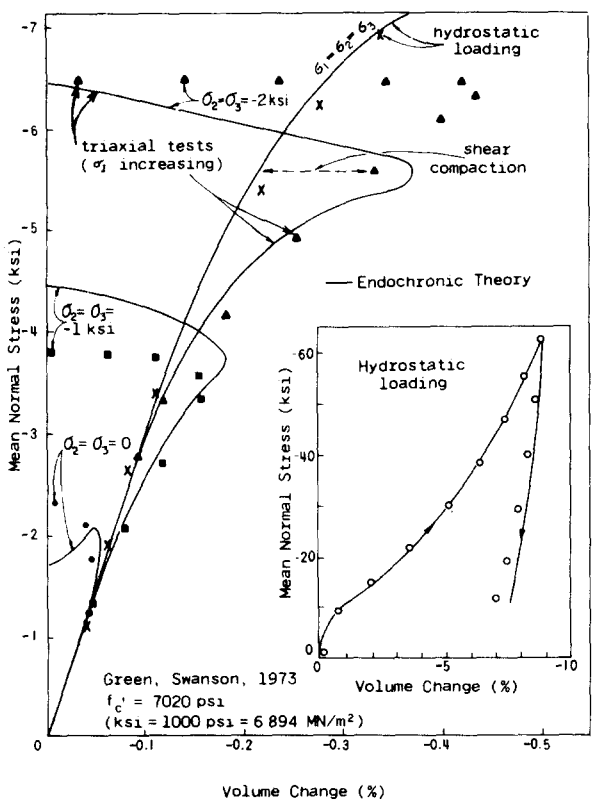

Fig. 8. Fit of Green and Swanson's data on volume change in hydrostatic loading and unloading and in triaxial tests.

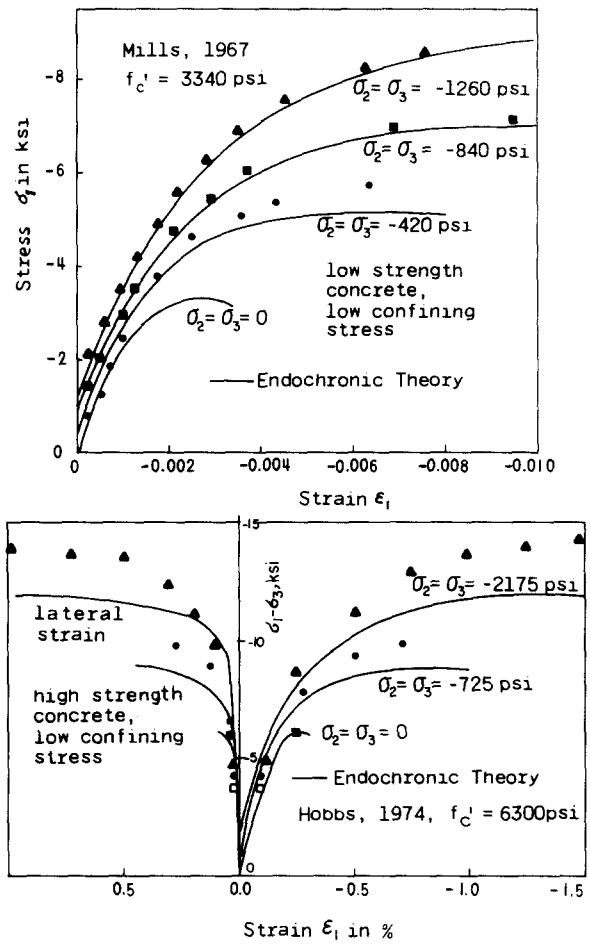

Fig. 9. Fit of Mills' and Hobbs' data on low strength concrete and high strength concrete at low confining pressures.

tion and for a discussion of the role of basic parameters. Only those aspects which are different from ref. [2] will be discussed herein.

The previously developed endochronic stress-strain relations for concrete [2] did not involve volumetric inelastic strains $d\epsilon''$ due to hydrostatic stress $p(Z_2 \to \infty, z' = \xi' = 0)$ and the expressions for their softening function $F(\boldsymbol{\varepsilon}, \boldsymbol{\sigma})$ were considerably simpler. In the present model, $d\epsilon''$ due to p is taken into account. For this purpose a second intrinsic time variable, called compaction measure ζ', is introduced here. Its purpose is to model inelastic volume change due to hydrostatic stress, which has been neglected in ref. [2]. This effect is important only at high hydrostatic pressures. From the shape of the hydrostatic loading and unloading

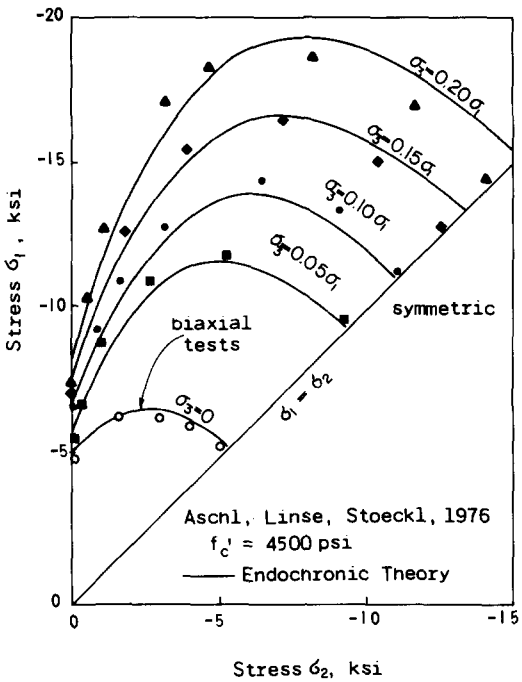

Fig. 10. Fit of triaxial failure envelopes for proportional loading tests of Aschl, Linse and Stöckl.

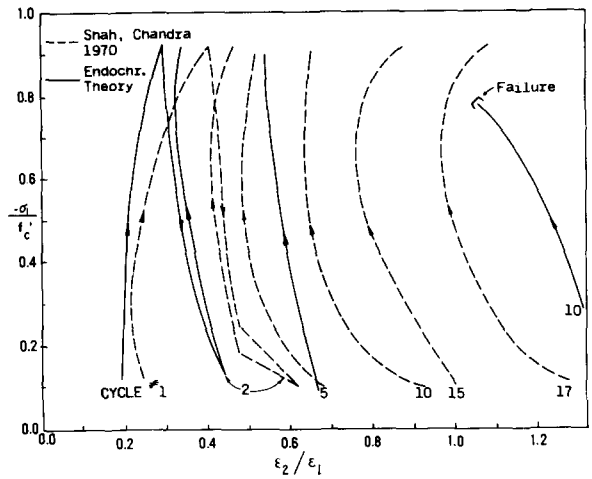

Fig. 12. Fit of Shah and Chandra's data on ratio of lateral to axial strains in uniaxial tests at high stress.

curves shown in figs. 8 and 6, it is apparent that the hydrostatic stress–strain relation is curved and irreversible, and that the unloading curve is initially at least as steep as the initial loading slope (see fig. 8). For such a behavior, the endochronic formulation is suitable. The softening function $H(\sigma)$ increases the inelastic volume change if the hydrostatic compression grows but becomes constant at higher compression levels. The less inclined medium portion of the hydrostatic curve is governed by the linear term in $h(\eta')$, and the subsequent stiffening is achieved by the quadratic term in $h(\eta')$.

Variable λ' represents the shear compaction which appears at the beginning of inelastic deformation, as is sketched in fig. 1d and confirmed by test data in fig. 8; (it is also encountered in sands). The function $l'(\lambda')$, eq. (18), prevents λ' from exceeding a certain limit, and the function $L'(\lambda', \boldsymbol{\varepsilon}, \boldsymbol{\sigma})$ causes $d\lambda'$ to vanish for large shear strain (large $J_2(\boldsymbol{\varepsilon})$) and also for all compression tests but the triaxial ones ($\sigma_{min} \neq 0$).

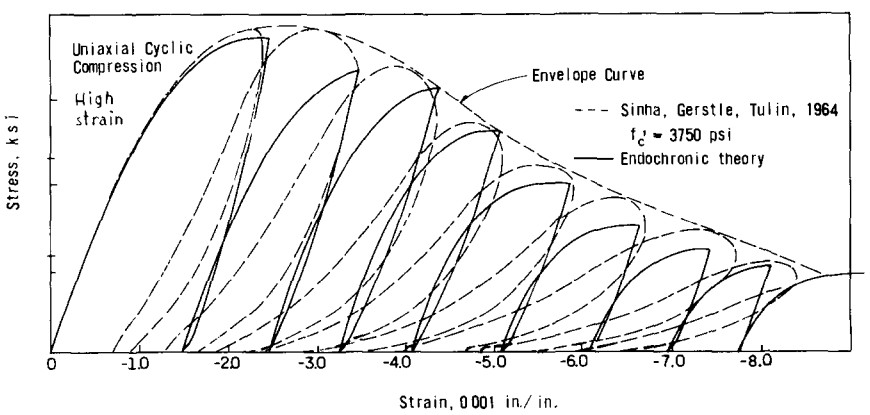

Fig. 11. Fit of Sinha, Gerstle and Tulin's data on unloading and hysteresis loops in the strain–softening range.

(This is not quite true for uniaxial data in fig. 5, but the fitting error is small.) For triaxial tests in which σ_{min} is tension, L' makes $d\lambda'$ positive (dilatancy). By contrast to dilatancy λ, compaction λ' is assumed to have no effect on elastic moduli G and K_1, eq. (17), since it is not associated with opening of pores such as cracks.

Coefficient F_4 in eq. (9) serves the purpose of shifting down the tail of the softening branch in biaxial compression; see fig. 1b and the resulting fit in fig. 4. Coefficient F_5 in eq. (9) adjusts the triaxial response curves at large strains; it shifts the end of the curve downward when the confining pressure p is high, and shifts the end upward when p is very low; see fig. 1e.

Coefficient g_1 controls the differences between the standard triaxial tests, for which $\sigma_{22} = \sigma_{33} =$ constant and σ_{11} grows, and the proportional triaxial tests, for which all stresses are increased keeping the ratio $\sigma_{11} : \sigma_{22} : \sigma_{33} =$ constant. Note that g_1 is zero for standard triaxial tests ($\sigma_{med} = \sigma_{min}$), as well as for uniaxial compression tests ($\sigma_{med} = \sigma_{min} = 0$) and biaxial compression tests ($\sigma_{min} = 0$).

Due to g_{11}, the value of coefficient g_1 increases with σ_{med} in proportional triaxial tests, and due to g_{12}, coefficient g_1 increases in these tests also with σ_{min}; see fig. 1a. Coefficient g_2 has the purpose of adjusting the response curves in proportional triaxial tests with low σ_{min} and standard triaxial tests with low confining pressure $\sigma_{min} = \sigma_{med}$; see fig. 1g.

Corrections furnished by coefficients g_1 and g_2 are mainly needed to obtain the correct peak stress values and the corresponding triaxial failure envelopes for proportional triaxial tests [7] (such tests have just been completed in Munich); see fig. 10. Without these corrections, the peak stress values would deviate considerably from test results, even though the standard triaxial tests are represented well even without g_1 and g_2. The inelastic dilatancy, λ (fig. 1c), is of the same form as before [2], but the values of coefficients have been altered. The dependence of G and K upon dilatancy λ is similar as before [2], but the expression is different [eq. (4.17)], yielding a slower decrease of G and K with λ at high λ (fig. 4.1h), such that G and K cannot become negative for any λ. This variation of G and K agrees with the observations based on energy dissipation [8,9].

By contrast with the previous formulation [2], the present one gives reasonable shapes of strain softening branches up to very large strains in uniaxial as well as biaxial and triaxial tests. Previously [2], the ends of these curves were too high in uniaxial and biaxial tests (figs. 2 and 3), and did not give a long flat plateau in triaxial tests at moderate p, as in fig. 1e.

The response curves have been also considerably improved for cyclic uniaxial tests at very large strains producing progressive deterioration of strength. The peaks of the subsequent hysteresis loops now decline in good agreement with test data (fig. 11). Nevertheless, the model is not yet perfect in that the area of the loops (fig. 1d) after several cycles is much too small and the mean slope of loops is not declining with the number of cycles as strongly as test data indicate (fig. 11).

The dependence of material parameters on strength f'_c is improved. This enabled adequate representation of triaxial test data for concrete of various strengths; see figs. 6–10. The fact that the peak stress point in uniaxial tests shifts to larger strains as lower strength is considered is also properly represented (fig. 2).

All test data fitted in ref. [2] and not shown here are represented by the present formulation at least as closely as in ref. [2].

4. Application in finite element analysis

A numerical algorithm for solving an incrementally loaded concrete structure with the help of the endochronic constitutive relation has been presented in ref. [2]. The algorithm uses central difference formulas for the increments of stresses and strains and employs iterations at each loading step. This algorithm has been applied in conjunction with the finite element method to predict the response of cylindrical specimens in double punch bearing stress tests, in which the load is applied only over a portion of the area of the end of the specimen. This is a problem of considerable practical importance, which has been extensively studied [10–14], and it is a problem in which a good constitutive relation that works both at small and high confining pressures is necessary. Therefore, endochronic theory seems particularly suited for solving this type of problem.

The endochronic theory as presented here does not

apply for tensile cracking. An extension to include gradual tensile cracking is possible – see F_3 in eq. (11) of ref. [2] – but it is more realistic to introduce an independent criterion for tensile cracking. This approach is widely used for the analysis of concrete structures and one recent version [15] has been applied here. Distributed cracks, normal to the direction of maximum principle tensile stress, are assumed to occur when the tensile strength, f_t', is reached. The cracking criterion is checked at every iteration of the loading step, and the incremental properties are revised according to the latest preceding iteration. The matrix of incremental elastic moduli is then modified [15] and becomes orthothropic, with zero stiffness in the direction normal to the crack. The original stress which is released by the cracking is distributed to other finite elements by

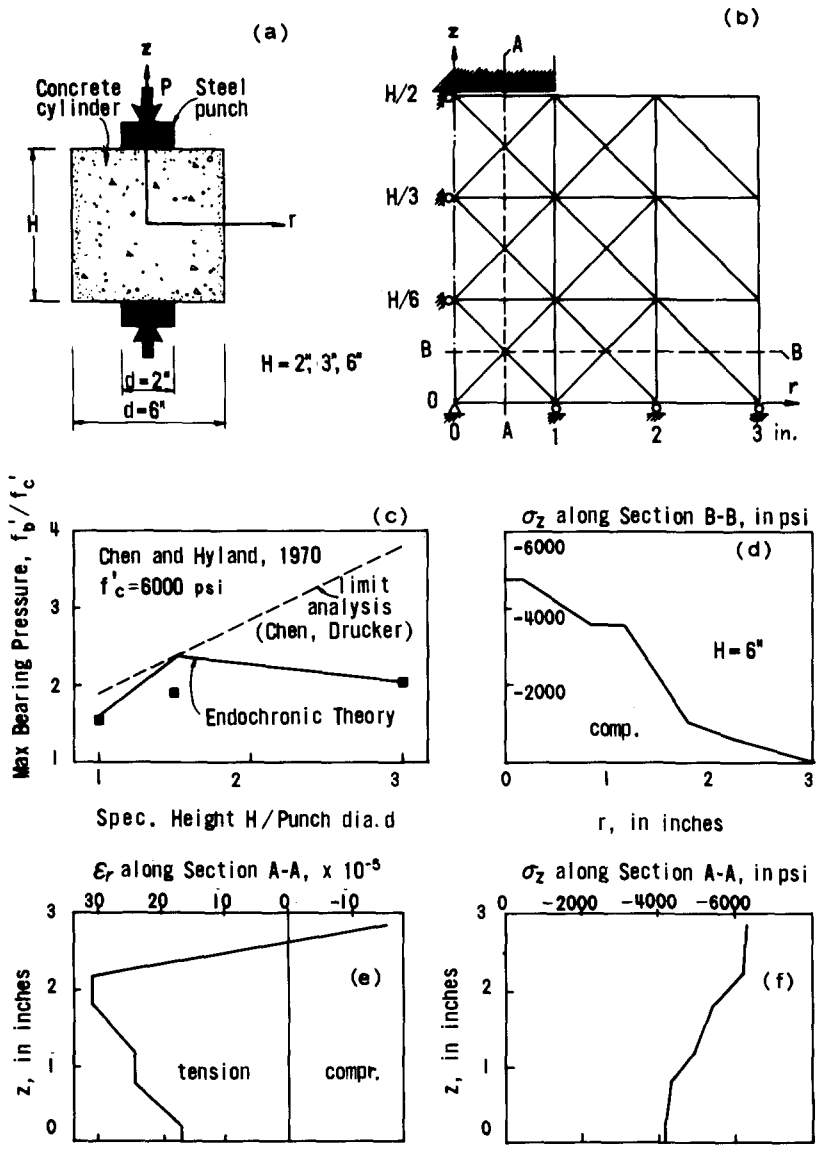

Fig. 13. Chen and Hyland's double punch bearing stress test (a); finite element grid used (b); comparison with test results (c); and calculated stress and strain distributions in typical cross sections (d–f).

applying equivalent nodal forces at the nodes of the element. A second system of cracks may form subsequently, being assumed to be normal to the first system. The shear transfer factor across the cracks, due to aggregate interlock, is taken to be 0.5. Since, in cracked concrete, large compressive stresses may develop in the directions parallel to cracks, the endochronic relations with the inelastic strains are used even for cracked concrete.

The test data chosen for comparison with the prediction are the sets no. 17, 18 and 19 from ref. [16], which reports bearing tests of cylinders having a diameter of 6 inches (152 mm) and lengths of 6 inches (152 mm), 3 inches (76 mm) and 2 inches (51 mm). The diameter of the steel punches, considered as rigid, is 2 inches (51 mm). Concrete is of compression strength $f_c' = 6000$ psi (41.36 MN/m^2) and tensile strength $f_t' = f_c'/12$. The finite element mesh used is shown in fig. 13b. Owing to symmetries, only one quarter of the axial cross section has to be analysed. Finite elements are chosen as three-node axisymmetric triangular ring elements [17]. Stresses are evaluated for the centroids of the elements and the cracking criterion is checked only for the centroids. The boundary condition under the punch was considered as a smooth sliding contact.

The results of the finite element analysis are plotted in fig. 13c for various lengths of specimen. Also shown are the results for elastic perfectly plastic limit analysis [18]. It can be seen that the endochronic theory gave distinctly better predictions of failure loads. The deviation for mean length specimens might be due to friction under the punches, whose value is uncertain. The calculated distributions of stress and strain in typical cross sections of the specimen are shown in figs. (13d–f). The corresponding measurements are not available.

5. Conclusion

The present refinement of the endochronic theory of concrete consists mainly in taking into account: (a) the inelastic strains due to hydrostatic compression; (b) improved descriptions of strain-softening behavior, (c) cyclic loading in strain-softening range, and (d) volume change in strain-softening range; (e) the differences between proportional and standard triaxial tests; (f) triaxial failure envelopes; and (g) dependence of material parameters on strength. The formulation consists fully of continuous functions, and for numerical analysis it has the advantage that it contains no inequalities.

The present expressions are, admittedly, rather complicated and contain many parameters. However, for computer calculations this is not an insurmountable drawback. The agreement with test data is far superior to any other constitutive law found this far – virtually all currently known basic properties are modeled (see also ref. [2]). The value of all material parameters are given, their dependence on concrete strength is identified, and a broad range of normal weight concrete is covered. Nevertheless, it is hoped that some day another formulation which would be at least as powerful but simpler than the present one will be discovered. It should also be expected that some significant disagreement with test data will be found when good experimental information on non-proportional loading paths becomes available.

References

[1] Z.P. Bažant, Proc., Soc. of Engng. Science 11th Annual Meeting, G.J. Dvorak, ed. (Duke University, Durham, N.C., 1974) p. 158.
[2] Z.P. Bažant, P. Bhat, J. Eng. Mech. Div., Proc. Am. Soc. Civil Engrs. 102 (1976) 701.
[3] Z.P. Bažant, P. Bhat, J. Struct. Mech. Div., Proc. Am. Soc. of Civil Engrs. 103 (1977) 153.
[4] Z.P. Bažant, A.A. Asghari, J. Eng. Mech. Div., Proc. Am. Soc. of Civil Engrs. 103 (1977) No. EM1.
[5] K.C. Valanis, Archiwum Mechaniki Stossowanej 23 (1971) 517.
[6] J.E. McDonald, Techn. Report C-75-4, Concrete Laboratory, U.S. Army Engineer Waterways Experiment Station, Vicksburg, Miss., Oct. 1975 (prepared for Oak Ridge Nat. Lab., ORNL-TM-5052/UC-57).
[7] H. Aschl, D. Linse and S. Stoeckl, private communication, Technical University, Munich, Aug. 1976.
[8] J.W. Dougill, J.C. Lou, and N.J. Burt, paper presented at the ASCE Speciality Conference on Mechanics in Engineering, University of Waterloo, Ontario, Canada, May, 1976; to appear in J. Eng. Mech. Div. ASCE.
[9] D.C. Spooner, C.D. Pomeroy and J.W. Dougill, Magazine of Concrete Research 28 (1976) 21.
[10] T. Au, and D.L. Baird, J. Concrete Institute, 56 (1960) 869.
[11] N.M. Hawkins, Magazine of Concrete Research, London, England, 20 (1968) 31.
[12] G.G. Meyerhof, Magazine of Concrete Research, April (1953) p. 107.
[13] S.K. Nigogi, J. Structural Division, ASCE 99 (1973) 1471.
[14] W. Shelson, J. Concrete Institute 54 (1957) 405.

[15] M. Suidan and W.C. Schnobrich, J. Structural Division, ASCE, 99 (1973) 2109.
[16] W.F. Chen and M.W. Hyland, J. Concrete Institute 67 (1970) 228.
[17] O.C. Zienkiewicz, (McGraw-Hill, London, 1971).
[18] W.F. Chen and D.C. Drucker, J. Engineering Mechanics Division, Proc. ASCE 95 (1967) 955.
[19] G.G. Balmer, Structural Research Laboratory Report No. Sp-23 (United States Department of the Interior, Bureau of Reclamation, Denver, Colorado, October, 1949).
[20] S.J. Green and S.R. Swanson, Technical Report No. AFWL-TR-72-2, Terra-Tek, Inc., Salt Lake City, Utah, April, 1973.
[21] D.W. Hobbs, Technical Report, Cement and Concrete Association, London, England, July, 1974.
[22] E. Hognestad, N.W. Hanson and D. McHenry, J. Concrete Institute, Proceedings 52 (1955) 455.
[23] H. Kupfer, H.K. Hilsdorf, and H. Rüsch, J. Concrete Institute, Proceedings 66 (1969) 656.
[24] L.L. Mills, Ph.D. Dissertation, New Mexico State University, Las Cruces, New Mexico, December, 1967.
[25] S. Popovics, Cement and Concrete Research 3 (1973) 583.
[26] S.P. Shah, and S. Chandra, J. Materials 5 ASTM (1970) 550.
[27] B.P. Sinha, K.H. Gerstle and L.G. Tulin, J. Concrete Institute, Proceedings 61 (1964) 195.